Chemical bonding and electronic properties of the Co adatom and dimer interacting with polyaromatic hydrocarbons

Mehdi Mahmoodinia,[†] Per-Olof Åstrand,[*,†] and De Chen[‡]

Department of Chemistry, Norwegian University of Science and Technology (NTNU), N-7491 Trondheim, Norway, and Department of Chemical Engineering, Norwegian University of Science and Technology (NTNU), N-7491 Trondheim, Norway

E-mail: per-olof.aastrand@ntnu.no

Abstract

The density functional calculations presented here elucidate the nature of the interaction between the Co atom and dimer with a polyaromatic hydrocarbon (PAH). The results are analyzed in terms of structural, electronic and magnetic properties. The bonding character of the Co atom and dimer adsorbed on the PAH exhibits a strong covalent bonding, arising from a hybridization between the d orbitals of Co and the p_z orbitals of the carbon atoms, which cause an in-plane distortion in the PAHs. A small charge transfer takes place from the Co atom and dimer to the PAH surface, which creates a positive charge on the metal atoms and thereby change their catalytic activity. Upon adsorption, the magnetic moment of the Co adatom is reduced depending on the adsorption site. For the perpendicular Co dimer to the PAH plane, the projected magnetic moment of the Co atom further from the PAH is increased, which is due to antiferromagnetic coupling between the Co atoms in this configuration. Density of state analysis shows that the main contribution of magnetic moment reduction is due to promotion of electrons from the $4s$ states to the $3d$ states of the Co adatom upon adsorption.

Keywords: Co particles, PAH, Charge transfer, Magnetic properties, ZORA

Introduction

Graphene is a two-dimensional honeycomb lattice[1–3] with superior properties such as high surface area,[4] linear dispersion of electronic states at the Fermi level,[5] semiconductor with zero bandgap,[6] superior electric conductivity and high thermal stability[7] which makes this material very attractive for many different potential applications ranging from future electronics to sensitive gas sensors.[8] Graphene has also attracted great attention as a support material for transition metal clusters,[9–17] since it is sufficiently inert and does not change the physi-

cal and chemical properties of the transition metal clusters by too much, but on the other hand it can stabilize the metal particles, increase the surface-to-volume ratio and therefore the catalytic activity of metal clusters.

Transition metal (TM) clusters have been the subject of intense efforts to adapt them for a variety of promising applications in different areas of nanotechnology from heterogeneous catalysis[18–21] to nano-magnetic devices.[22–24] There are several theoretical and experimental efforts devoted to understanding the structural, electronic, and magnetic properties of TM clusters.[25–35] In particular, Co clusters are one of the most important examples due to their magnetic properties[31–36] and their importance in the Fischer-Tropsch (FT) process.[37–40] Due to the high activity and long life time,[36] cobalt-based catalyst is currently the catalyst of choice for the conversion of syngas to liquid fuels in the FT process. Cobalt and cobalt-oxide nanoparticles on graphene can catalyze the oxygen reduction reaction nearly as well as platinum does and is substantially more durable.[41] Hence, more effort is needed to improve the efficiency and catalytic activity of these catalysts. Analysis of the interaction between the atoms at the interface is essential for gaining a better insight of the properties of these catalysts on the atomic level.

The interfaces between TMs and graphene have been investigated widely.[42–58] For example, we have recently studied the interactions between the Pt adatom and dimer and PAH surface, where it turns out that the electron transfer between the metal and the surface is substantial.[42,59] We have shown that the magnitude of charge transfer and the adsorption energy of the Pt atoms and dimers bound to PAH depend upon the adsorption site and adsorption configuration. Sevinçli et al.[14] investigated the electronic and magnetic properties of graphene and graphene nanoribbons functionalized by $3d$ TM atoms. They found that $3d$ TM atoms can be adsorbed on graphene with binding energies ranging between 0.10 and 1.95 eV depending on the species

and coverage density. The structural and electronic properties of zigzag graphene nanoribbon (ZGNR) with the adsorption of Co and Ni have been investigated by Wang et al.[52] and they found that the interaction between the Ni atom and the ZGNR is stronger than the interaction for the Co atom. By using scanning tunneling microscopy (STM) and X-ray photoelectron spectroscopy, Müller et al. investigated Pt clusters on the basal plane of highly oriented pyrolytic graphite.[48] While Rigo et al.[60] and Chan et al.[11] suggested a chemisorption between the $3d$ TMs and the graphene surface, Johll et al.[10] discussed physisorption of TM clusters on graphene. These investigations mostly focus on the stability, energetic and magnetic properties of TMs adsorbed on the graphene surface. One of the most important aspects in the chemistry of the TM-graphene interface, which is still to a large extent unexplored, is tailoring the spin state and electronic structure of TM clusters on the graphene surface. Therefore, this paper is also devoted to investigate the spin state and electronic structure changes by adsorbing the Co atom and dimer on the PAH surface. Density functional theory (DFT) is a successful approach for the description of the ground-state properties of TMs and also study their interaction with graphene surface at the atomistic level.[11–17] When considering this type of interaction, however, the effect of dispersion forces becomes important.[61–66] Grimme's dispersion correction[67,68] has been demonstrated to successfully stabilize the adhesion of a graphene layer on a Ni(111) substrate[69] and adsorption of Pt atom and dimer on graphene surface.[42] Furthermore, for a correct description of heavier elements with $Z \geq 20$, relativistic effects become important.[70,71] Hence, the scalar and full ZORA approches are used to treat relativistic effect.[72–77]

Graphene is an ideal system whereas real systems include defects, and therefore a realistic description of the adsorption of the Co atom and dimer on the graphene needs a proper model to represent the graphene surface. Polyaromatic hydro-

carbons (PAHs) have been successfully utilized as model systems for graphene[42,59,78–80] and are considered as model structures for the adsorption of the Co atom and dimer on graphene in this study since bonding to PAHs represents a model for binding to the π system relatively near defects in a real graphene material.

Therefore, in this study the stability, electronic and magnetic properties of Co adatom and dimer adsorbed on PAH surface at several different adsorption sites and for different spin states are investigated. Furthermore, to elucidate the nature of these interactions, we analyzed the density of states obtained from spin-polarized DFT calculations.

Computational details

In the present work, calculations have been carried out by the Amsterdam Density Functional (ADF) code.[81,82] All calculations were performed with the ZORA approach to include relativistic effects and spin-obit coupling effects were also studied using the fully relativistic ZORA approach. The S12g functional[83] is used as the exchange-correlation functional, which is the successor of the Swart-Solà-Bickelhaupt (SSB-D) functional,[84,85] correcting some shortcomings of the SSB-D functional in the exchange part and it also includes a more recent dispersion correction (Grimme's D3).[86] Its performance for spin states of transition metal complexes is well documented.[83,87] For comparison, the Perdew-Burke-Ernzerhof (PBE) functional[88] has also been employed in our study.

The molecular orbitals (MOs) are expanded in an uncontracted set of Slater-type orbitals (STOs) and Slater-type functions are substantially more diffuse than a corresponding Gaussian type basis set and give consistent and rapidly converging results, which may be related to the cusp at the nuclei that is correctly described by STOs.[89] Since some orbitals become almost linearly dependent, a few orbitals are removed during the calculation.

Polyaromatic hydrocarbons (PAH) were chosen to model a graphene surface because of the similarity of the electronic structure between the graphene[90,91] and the PAHs.[92–94] To find a representative size for predicting the adsorption energy of the Co atom, different PAHs were tested. The size of molecules ranges from benzene (C_6H_6) to circumcircumpyrene ($C_{80}H_{22}$) (see Fig. 1). Finally, the $C_{54}H_{18}$ molecule (circumcoronene) is selected as a suitable model.

Geometry optimizations were performed with the Broyden-Fletcher-Goldfarb-Shanno (BFGS)[95] algorithm with a convergence criterion of 10^{-6} a.u. on the energy and the charge density. In the geometry optimizations, we first impose constraints for the x and y coordinates of the Co atom and dimer to keep them in the expected binding site and relaxing the distance along the z-axis (perpendicular to the PAH plane). Then the geometry was relaxed without constraints to find the most stable geometry. Moreover, a frequency analysis was carried out to ensure that the stationary points are either minima (only real frequencies) or transition states (one imaginary frequency).

The relative stability of Co_n-PAH complexes are determined by the adsorption energies, in which a more negative value of the adsorption energy indicates a stronger binding of the adatom to the PAH surface. The adsorption energy, E_{ads}, is thus defined as

$$E_{ads} = E_{Co_n/PAH} - E_{PAH} - nE_{Co} \qquad (1)$$

where $E_{Co_n/PAH}$, E_{PAH} and E_{Co} are the ground state energies of the Co_n/PAH system, the PAH molecule and an isolated Co atom, respectively. We also defined the interfacial interaction energy, E_{int}, as

$$E_{int} = E_{Co_2/PAH} - E_{PAH} - E_{Co_2} \qquad (2)$$

where E_{Co_2} is the total energy of the Co dimer in the gas phase. The interfacial interaction energy measures the interaction energy of the dimer with the PAH surface, and consists of a negative contribution from the energy gained by forming Co_2-PAH bonds

and positive contributions from the distortions of both the Co dimer and the PAH molecule. The basis-set superposition error (BSSE) was included using the counterpoise method.[96]

To check the effect of the electronic structure on Co-PAH interactions, several spin states for the Co_n-PAH (n = 1, 2) complex are studied with the S12g functional, which has been demonstrated to be successful for describing spin states of transition-metal complexes.[83,87] Many standard density functionals fail to predict the spin ground-state of transition-metal complexes[97] and the S12g functional was specifically designed to do well in this respect.[83] The spin state is denoted with the spin multiplicity, $2S + 1$, which is for example, 1 for a singlet state, 2 for a doublet state and 3 for a triplet state and so on. The degree of spin contamination for a spin-unrestricted calculation is checked by evaluation of the $< S^2 >$ values, which ideally should be $S(S + 1)$ and thereby 0.00 for a singlet, 0.75 for a doublet, 2.00 for a triplet, 3.75 for a quartet, 6.00 for a quintet and 12.00 for a septet state.

The atomic charges are calculated by the Hirshfeld charge analysis[98,99] which is evaluated by numerical integration in ADF, and appear to be reliable and not very sensitive to basis set effects.[81] Mulliken population analysis[100,101] is used to estimate the average spin density in order to determinate the contribution of each Co atom to the total magnetic moment.

Results and Discussion

Basis set study

To select a proper basis set to describe our system, we did a basis set study using different basis sets and the S12g functional on the Co-coronene complex (See Table 1). The coronene molecule has been successfully used as a graphene model in several theoretical investigations.[78–80] According to our

Table 1 Adsorption energies without, ΔE, and with the BSSE correction, ΔE^{CP}, and the BSSE contribution for the Co-coronene complex with different basis sets. Basis sets before / are for the C and H atoms, and basis sets after the / are for the Co atom. In the TZ2P.1s and QZ4P.1s basis sets, the $1s$ core shell is kept frozen for the C atoms. In the TZ2P.2p basis set, the core shells up to $2p$ are kept frozen for the Co atoms.

Basis set	ΔE (eV)	BSSE (eV)	ΔE^{CP}(eV)
DZP / TZP	-1.45	0.31	-1.14
TZP / TZP	-1.31	0.61	-0.70
TZ2P.1s /TZ2P.2p	-1.05	0.30	-0.75
TZ2P.1s / TZ2P	-0.84	0.08	-0.76
TZ2P / TZ2P	-0.82	0.08	-0.74
TZ2P.1s / TZ2P+	-1.02	0.21	-0.81
TZ2P / TZ2P+	-1.01	0.20	-0.81
TZ2P.1s / QZ4P	-1.00	0.07	-0.93
QZ4P.1s / QZ4P	-1.04	0.11	-0.93
QZ4P / QZ4P	-1.02	0.07	-0.95

basis set study, the QZ4P basis set,[102] which has triple-quality in the core and quadruple-quality in the valence orbitals, and containing four sets of polarization functions, is needed to describe the Co atom, and the TZ2P basis set[102] which has double-quality in the core and triple-quality in the valence orbitals and containing two sets of polarization functions, is sufficient to describe the C and H atoms. The $1s$ core shell is kept frozen for the C atoms to speed up the calculations without affecting the accuracy of the results. Basis set super position error is used to test the convergence of the basis set, which is small (0.07 eV) for the selected basis set, TZ2P.1s/QZ4P.

To investigate the contribution of relativistic effects in our calculations, we studied the adsorption of a single Co atom on the $C_{24}H_{24}$ molecule, using the scalar relativistic ZORA and the non-relativistic approach. The calculated adsorption energy using the S12g functional and the TZ2P basis set, is -0.82 eV for the scalar relativistic ZORA approach, and -1.15 eV for the non-relativistic approach, respectively, indicating that relativistic

effects are significant for the adsorption of the Co atom on the PAH surface. Therefore, the ZORA approach is included in this work.

Cobalt atom and dimer

Before discussing the geometric and electronic structure of the Co_n-PAH complexes, we first evaluate briefly the electronic structure of the Co atom and dimer since their characteristics have major influence on the properties of the Co_n-PAH complex. We also compare our results with the available experimental data and previous theoretical reports on the Co atom and dimers to validate how well our calculations estimate the binding energy, bond length, magnetic moment and ionization potential for the Co atom and dimer (see Table 2).

The experimental ground state of the cobalt atom is the quartet state ($4s^2 3d^7$ configuration) and the first two low-lying excited states identified as $4s^1 3d^8$ (quartet, $S = 3/2$) and $4s^1 3d^8$ (doublet, $S = 1/2$) configurations are higher in energy by 0.42 and 0.86 eV, respectively.[103] For the S12g functional, the quartet state ($4s^2 3d^7$) is also found to be the ground state of the cobalt atom and the first excited state (quartet, $4s^1 3d^8$) is calculated to be 0.39 eV higher in energy, which is in reasonable agreement with the experimental results. The doublet ($4s^1 3d^8$) and sextet states ($4s^1 3d^7 4p^1$) are higher in energy by 1.06 and 4.28 eV, respectively. The ground state of the Co dimer is a quintet state for both the PBE and S12g functionals which is in agreement with experimental[104] and other theoretical studies.[105–109] For the S12g functional, the septet, triplet and singlet states are higher states with 0.35, 1.30 and 2.66 eV excitation energy, respectively. For the PBE functional, the excitation energies are 0.37, 0.96 and 3.18 eV for the septet, triplet and singlet states, respectively. The ground state of the cation dimer is found to be a sextet state, in agreement with electron spin resonance spectroscopy.[110] There is a lack of experimental

studies on Co dimer and the existing experimental data for the binding energy are inconsistent. While a collision-induced dissociation experiment[111] predicted a value of less than 1.32 eV, a mass spectroscopic experiment[104] estimates a value of 1.69 ± 0.26 eV for the binding energy of Co dimer. The calculated binding energy for the Co dimer is 2.41 eV, which overestimate the latter experimental value by 0.55 eV, but within the range of $0.42-2.72$ eV for other theoretical studies.[105–109] The magnetic moment of the dimer was calculated for 2 μ_B per atom, which is in agreement with theoretical and experimental results.[104,106,107,109] We also calculated the IP of 6.87 eV (S12g) and 7.01 eV (PBE) for the ground state of the Co dimer which is in reasonable agreement with experiment[111] and other theoretical approaches.[105–107]

We have not found any experimental bond length for the Co dimer, except for an estimated bond length of 2.31 Å from the Pauling radii.[104] Our calculated bond length for the ground state of the Co dimer is 1.96 Å for both the S12g and PBE functionals, which is in between the experimental values obtained for the Fe_2 and Ni_2[112,113] and within the range of $1.95-2.41$ Å for different computational methods.[105–109]

The effects of the spin-orbit coupling are also studied for the Co dimer using a full relativistic ZORA approach. The equilibrium bond distance is calculated for 1.96 Å, as in the scalar relativistic approach, and the binding energy and IP are calculated to 2.48 and 6.83 eV, respectively, in agreement with the scalar ZORA approach. The projected electronic configuration and magnetic moment on each Co atom are calculated for $4s^{1.04} 3d^{7.85} 4p^{0.09}$ and 2 μ_B, respectively. However, there is no differences in the structural properties and small differences in the energetic and electronic properties of the dimer using the scalar and full ZORA relativistic approaches. Therefore to reduce the computational time we use the scalar approach in the remaining part of this work.

The bonding in transition-metal dimers can be de-

Table 2 Relative energy (E_{rel}, the energy relative to the lowest spin-state), binding energy (E_b), equilibrium bond lengths (R_e), ionization potential (IP), magnetic moments on atoms (μ_M) and effective atomic electronic configurations for different spin multiplicities (2S + 1) of the Co atom and dimer. The binding energy is computed for $E_b = 2E_{Co} - E_{Co_2}$ and the negative value indicates an unstable spin state for the Co dimer.

M	2S+1	E_{rel}(eV)	E_b(eV)	R_e (Å)	IP(eV)	μ_M (μ_B)	electronic configuration	Reference
Co	2	1.06			8.63	1.0	$4s^{1.00}3d^{8.00}4p^{0.00}$	
	4	0.00			8.71	3.0	$4s^{2.00}3d^{7.00}4p^{0.00}$	
	6	4.28			5.05	5.0	$4s^{1.00}3d^{7.00}4p^{1.00}$	
Co$_2$	1	2.66	-0.24	1.89	9.05	0.0	$4s^{1.00}3d^{7.93}4p^{0.06}$	
	3	1.30	1.11	2.03	6.90	1.0	$4s^{1.00}3d^{7.89}4p^{0.08}$	
	5	0.00	2.41	1.96	6.87	2.0	$4s^{1.00}3d^{7.92}4p^{0.07}$	
	7	0.35	2.06	1.99	8.67	3.0	$4s^{1.31}3d^{7.43}4p^{0.24}$	
Theoretical			2.26	2.01	7.48	2.0		Ref. [107][a]
			0.87	1.96	5.97	2.0	$4s^{0.87}3d^{8.06}4p^{0.07}$	Ref. [106][b]
			1.33	2.41		2.0		Ref. [109][c]
			0.81	2.56		2.0		Ref. [109][d]
Experimental			≤1.32		6.42			Ref. [111][e]
			1.69±0.26	2.31				Ref. [104][f]
					6.29±0.16			Ref. [114][g]

[a] GGA calculations using the exchange gradient correction of Perdew and Wang and the correlation gradient correction proposed by Perdew.

[b] Self-consistent spin polarized non-local generalized gradient approximation.

[c] Second-order Møller-Plesset perturbation theory.

[d] Multireference single- and double-configuration interaction molecularorbital theory.

[e] The collision-induced dissociation experiment.

[f] Using information derived from a combination of effusion and mass-spectrometric techniques. The equilibrium bond length is estimated based on Pauling radii.

[g] A procedure for the determination of metal cluster IPs using excimer laser lines.

scribed as a multiple bond formed between two atoms in a $d^n s$ state.[115] The Mulliken population analysis using the S12g functional gives a charge distribution of $4s^{1.00}3d^{7.92}4p^{0.07}$ for each Co atom in the neutral dimer which indicates that $3d$ orbitals participate in the bonding. This is in agreement with Jamorski *et al.*[107] where they suggest a triple bond for the Co dimer using the Mayer bond order analysis.[116] For carbon compounds, the results from bond order analysis can be explained by molecular orbital analysis as well, because of their covalent nature, but for the metal-metal bonding, because of orbital mixing, the situation is more complicated.

Graphene model

As seen in Fig. 1, eight molecules consisting of benzene, naphthalene, anthracene, coronene, circumanthracene, circumcoronene, circumovalene and circumcircumpyrene are used for modeling a part of a graphene sheet. The adsorption energies and the bond length of the Co-C bond for these PAH molecules are shown in Table 3. To find the adsorption energy of the Co atom, the Co atom is placed on the center of hexagonal ring (hollow site), which is the most favorable position for the Co atom.[117,118] The geometrical parameters of the PAHs were fully relaxed during the optimization. There is a notable correlation between the PAH size and the adsorption
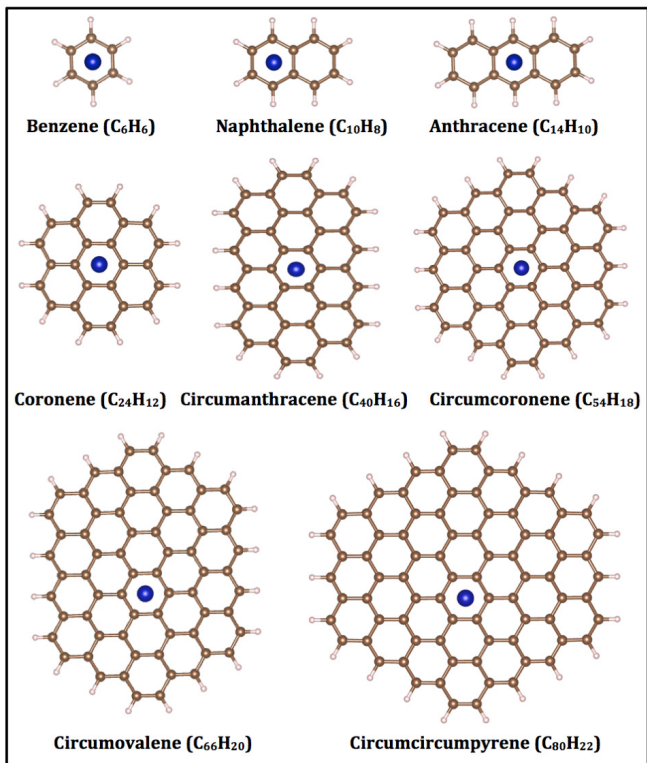
Figure 1 Molecules used in this study to represent the graphene sheet. The blue, brown and the pink circles indicate the Co, C and the H atoms, respectively.

energy. As observed from the Table 3, the adsorption energy tends to converge after circumcoronene ($C_{54}H_{18}$), and the size of this PAH molecule is sufficiently large in which the changes in the adsorption energy and Co-C bond distance are small. Therefore, the circumcoronene molecule was employed as the model for representing the graphene surface in this study. Indeed, this hexagonal nano-flake has attracted great interest with respect to its interesting properties like electronic absorption spectra,[119] and it has been successfully applied for modeling graphene in previous theoretical work.[120–124]

Several theoretical studies have focussed on acenes[125–127] and oligoacenes[128–132] using DFT and *ab-initio* methods. However, because of the polyradical character of oligoacenes,[125,126] the spin ground state of these molecules have to be checked. Singlet-triplet (S-T) excitation energies give valu-

Table 3 Adsorption energies, E_{ads}, and equilibrium distance, d_{Co-C}, for adsorption of the Co atom on different PAH molecules.

Molecule	E_{ads}(eV)	d_{Co-C}(Å)
C_6H_6(Benzene)	-1.56	2.00
$C_{10}H_8$ (Naphthalene)	-1.48	2.01
$C_{14}H_{10}$ (Anthracene)	-1.39	2.02
$C_{24}H_{12}$ (Coronene)	-1.14	2.08
$C_{40}H_{16}$ (Circumanthracene)	-1.12	2.09
$C_{54}H_{18}$ (Circumcoronene)	-1.04	2.08
$C_{66}H_{20}$ (Circumovalene)	-1.01	2.09
$C_{80}H_{22}$ (Circumcircumpyrene)	-0.99	2.08

able information about the spin ground state of these compounds, and several theoretical groups have reported the S-T[127,133] and the singlet-singlet (S-S)[134] excitation energies of these molecules. Rayne and Forest[133] reported a triplet state as ground state while Bendikov *et al.*[125] and Tonshoff *et al.*[135] found a singlet state for the ground state of nonacene. Multireference averaged quadratic coupled cluster theory[127] also suggested the singlet state for the ground state of the small acenes (up to n=13), however by comparing with experimental data and applying a relative theoretical-experimental error (0.27±0.06 eV), a quasi-degenerate singlet and triplet state is suggested for the larger acenes ($n \geq 11$). Wang *et al.* reported an open-shell singlet state for the 5a5z periacenes, but degenerate singlet-triplet state for the 6a6z periacene, using R(U)B3LYP/3-21G.[136] Accordingly, we investigated the electronic ground state of our PAH model ($C_{54}H_{18}$) by time-dependent DFT.[137] The first S-S and S-T excitation energies were calculated to 1.94 and 1.77 eV, respectively. The positive S-T splitting indicated that the system maintains a singlet ground state character for this computational level. We also did a geometry optimization of the triplet state of the PAH (assuming that the triplet state would be just above the open-shell singlet state if the singlet di- or poly-radical is the ground state) and found that the triplet state is 1.69 eV higher

than the closed-shell singlet state. Furthermore, we also investigated the open-shell singlet state using the spin-flip approach[138] and found that the closed-shell singlet state is only 0.006 eV higher than the open-shell singlet state. Still, the spin ground-state needs to be verified for each PAH system studied.

To better understand the electronic structure of the PAH molecule, we also studied the density of state (DOS). The DOS plotted in Fig. 2 shows the total density of state (TDOS) of the PAH molecule and the partial density of states (PDOS) for the C and H atoms. Fig. 2a, shows a vanishing density of
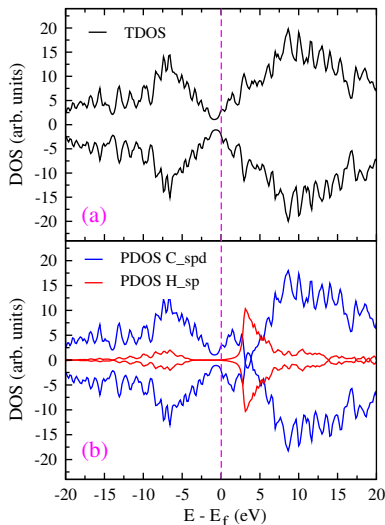

Figure 2 (a) Total density of state (TDOS) of the PAH molecule, and (b) the partial density of states (PDOS) of its individual contributions from the C and H atoms.

states at the Fermi energy, as for a single graphene sheet.[139] The majority (spin up) and minority (spin down) states of the PAH molecule are completely symmetric resulting in zero net magnetic moment. It has been presented in the literature that adsorption of H atom on graphene lattice can induce a magnetic moment about $1\mu_B$, and possibly to be ferromagnetic when two H atoms are located on the same sublattice of graphene,[140–142] but a pair of hydrogen atoms that are located on the different sublattices of graphene cannot induce magnetic moment.[143,144] The Fermi level is moved upward from the graphene Dirac point,[145] due to electron transfer

from H atoms, which saturating the open ends of the sheet. Fig. 2b shows the individual contributions from the C and H atoms of the PAH surface. The PDOS of the C atoms are more like the electronic structure of the graphene sheet, but overlap between the states of C and H atoms create a gap in the Dirac point of the C sheet, which appears in the TDOS of the PAH molecule.

Cobalt atom on the PAH surface

We consider the binding of the Co atom on three highly symmetric adsorption sites: the top site, above a carbon atom, the bridge site, between two neighboring carbon atoms, and the hollow site, surrounded by six carbon atoms (see Fig. 3). There are several possibilities and initially we looked at many more adsorption configurations, but we only present three positions as representative of bridge, top and hollow sites.

The adsorption energies, Co-C bond distances, magnetic moment on the Co atom and the Hirshfeld atomic charge for the Co atoms for different spin states and for the three structures in Fig. 3 are given in Table 4. The Co-C bond distance is the average distance between the Co atom and its nearest carbon atoms for the bridge and hollow sites since the structures are not entirely symmetric. The most stable configuration for the binding of the Co atom to the PAH surface is the hollow site, followed by the bridge and the top sites, respectively. The results are based on fixing the position of the Co adatom along the x- and y-axes, i.e. in the surface plane, and relaxing the distance along the z-axis (perpendicular to the PAH surface). However, after a complete relaxation of geometry, the Co adatom moves across the top and bridge sites toward the hollow site, showing the bridge and top sites may not be minimum points on the potential energy surface. To identify the nature of the stationary points, the vibrational frequencies are computed. There is no imaginary frequency for the hollow configuration, showing it is a minimum on the potential energy surface. A single
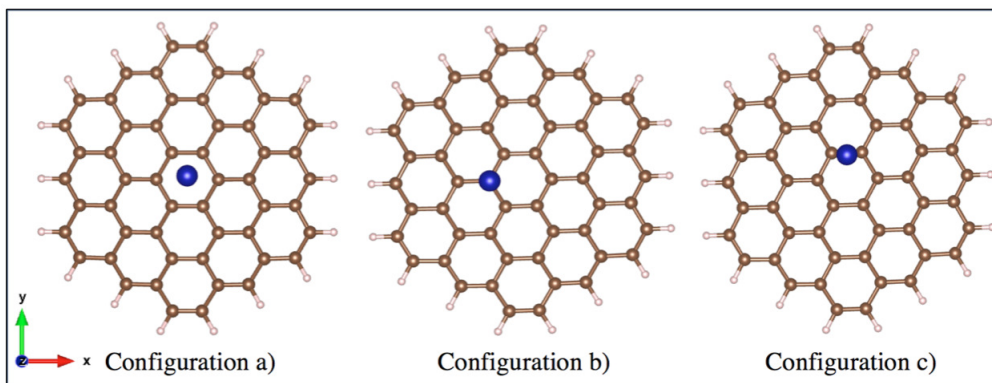
Figure 3 Stable configurations for the Co atom adsorption on the $C_{54}H_{18}$ molecule. The configurations *a*, *b* and *c* are the hollow, top and bridge sites, respectively. The blue, brown and pink circles indicate the Co, C, and the H atoms, respectively.

imaginary frequency of -66.89 and -76.50 cm^{-1} for the bridge and top configurations, respectively, indicate that they are not minima on the potential energy surface. This is in agreement with calculations by Jiménez-Halla *et al.* for the interaction of Cr(CO)$_3$ on a PAH fragment.[146] They found that the hollow site is a minimum and that the bridge and top sites are transition states.

Yazyev and Pasquarello[117] examined trends across the TM series and found that adsorption in a hollow site to be favored for most of the TMs, with the exception of the Ir, Pd, and Pt where the bridge site is favored. Dai et al.[118] also found adsorption to the bridge site to be favored for Pt clusters on a graphene surface. It seems like the hollow site is the preferred site for TM atoms with a partially filled d shell, while the bridge site is the most stable site for TM atoms with a filled or an almost filled d shell.

The adsorption of TMs on graphene differs from the adsorption of monovalent or closed-shell adsorbates, since the ground-state electronic structure of TMs undergoes several transitions upon adsorption.[78] In a previous work,[42] we found that when a single Pt atom approaches the PAH surface, its ground-state changes from triplet ($5d^9 6s^1$) to the closed-shell ($5d^{10} 6s^0$) singlet state. According to the results in Table 4, for adsorption of the Co adatom on the PAH surface, the doublet state is the electronic ground

Table 4 Results for the Co adatom adsorption on the $C_{54}H_{18}$ molecule with configurations according to Fig. 3. The adsorption energy (E_{ads}, in eV), the bond distance (d_{Co-C}, in Å), the magnetic moment (M, in Bohr magneton), the Hirshfeld atomic charge (e) of the Co atom and the $<S^2>$ values for different spin multiplicities (2S + 1) of the Co-PAH complex.

Config.	2S+1	E_{ads}	d_{Co-C}	M	Charge	$<S^2>$
Config. a)	2	-1.04	2.06	1.07	0.20	0.80
	4	-0.42	2.65	3.05	0.10	3.78
Config. b)	2	-0.45	1.86	1.12	0.27	0.81
	4	-0.43	2.03	2.87	0.09	3.80
Config. c)	2	-0.57	1.93	1.18	0.24	0.80
	4	-0.41	2.12	3.21	0.06	3.78

state, which means that upon adsorption of a Co atom, its most stable electronic structure undergoes a transition from quartet state ($3d^7 4s^2$ configuration) to the doublet state ($3d^9 4s^0$ configuration). This transition can be explained by ligand field theory.[147] When a Co atom approaches the PAH surface the $4s$ occupation becomes less favorable, because of the Pauli repulsion between a very diffuse $4s$ orbital of the Co atom and the π electrons of the PAH surface, and on the contrary the occupation of the $3d$ orbital becomes more favorable due to the shielding of the Coulomb repulsion in the $3d$ shell of the Co atom.[78] This is in agreement with previous studies

where it is found that the doublet state is the ground-state of Co/C complexes.[78,80,148] In this situation, the hybridization between the $3d$ orbitals of the Co atom, which is now become almost filled and the π^* orbitals of the PAH molecule is more feasible, because the $4s$ orbitals of the Co atom are almost empty and the atom-surface repulsion is therefore much weaker.

The adsorption energy for the Co adatom is found to be -1.04 eV for the hollow configuration, Fig. 3a, for the ground spin state ($3d^9 4s^0$) which is in range of the adsorption energy predicted by DFT studies (~1 eV). The quartet state ($3d^7 4s^2$) is higher in energy by 0.62 eV. The doublet-quartet separation is in close agreement with the experimental inter-configurational energy between the doublet and quartet states of a free Co atom of 0.86 eV,[103] and confirm this transition upon adsorption. The adsorption energy for the Co atom on the top and bridge sites (Figs. 3b and 3c) are -0.45 and -0.57 eV, respectively. Despite the fact that the interpretation of $<S^2>$ is not entirely straightforward for unrestricted DFT as in the case of UHF,[149] we checked the degree of spin contamination by comparing the expectation value $<S^2>$ with the ideal value, $S(S+1)$. Hence, the degree of spin contamination is calculated to be less than 10% for all relevant calculations, as seen in Table 4.

The Hirshfeld charge[98] analysis gives the effective charge transfer between the Co atom and the PAH surface. For all configurations we found that electrons are transferred from the Co atom to the surface, resulting in a positive charge on the Co atom. The magnitude of the charge is the largest for the top site (0.27 e) and the smallest for the hollow site (0.20 e). By comparing the Co-C bond distance and the charge transfer on different sites, the magnitude of the charge transfer decreases with Co-C bond elongation. This is consistent with the charge-transfer model based on a modified electronegativity equalization scheme,[150] where the amount of charge-transfer depends strongly on the bond length. The spin multiplicities have a large effect on both

structural and electronic properties of the Co-PAH complex. At all three different adsorption sites, the Co-C bond distance is increased due to increasing the Pauli repulsion between the $4s$ state of the Co atom, changing from the doublet to the quartet states, and the p_z orbitals of the PAH surface. Hence, the adsorption energies and the charge transfers indicate a significant decrease from doublet to quartet states. The Co-PAH interaction shows a physisorption character for the quartet state, in agreement with the potential energy curve obtained the by complete active space self-consistent field (CASSCF) approach,[78] which will be discussed later.

An important feature of the TM adatoms upon absorption on graphene is their different magnetic behavior.[151] The magnetic moment of the Fe atom is reduced by 2 μ_B[152] and the magnetic moment for the Mn atom is enhanced by 0.56 μ_B,[152] whereas the magnetic moment of the Cr atom does not change upon adsorption.[151] We therefore calculated the magnetic moment of the isolated Co atom and compared it with the corresponding value of the Co adatom on the PAH surface at different adsorption sites. The isolated Co atom at the ground state (quartet state) possesses the magnetic moment of 3 μ_B, which is larger than the magnetic moment of the bulk Co (1.73 μ_B/atom). This value is reduced upon adsorption on the PAH surface to 1.18, 1.12 and 1.07 μ_B, for the top, bridge and the hollow sites, respectively, and is thus dependent on the adsorption site. There might be two reasons for the reduction of the magnetic moment from the isolated to the adsorbed atom: one is the charge transfer between TM atom and the carbon surface, such as for the early transition metals like Ti and Zr, where ionic bonding is more prominent with a large amount of charge transfer from the adatom to the carbon.[153] The other reason is that electrons shift from one state to another state, such as for the middle transition metals like Fe,[152,153] Pt[42] and Co atoms, where the M-C bond has more covalent than ionic character with more hybridized states of carbon and adatoms. The interaction of the Co atom with the PAH surface is

chemisorption which involves a hybridization between the d orbitals of the Co atoms and the p_z orbitals of the carbon atoms, in agreement with previous studies.[12,145,154]

To further investigate the effects of metal binding to the PAH surface and understand the electronic structure of these systems, we analyzed the density of states obtained from the spin-polarized DFT calculations. The electronic structure of the PAH is strongly perturbed by "chemisorption" but it is essentially preserved in the weak binding "physisorption" regime.[145] Fig. 4 shows the TDOS and PDOS of the Co-PAH complex for the different adsorption sites. The electronic structure of the Co-PAH complex has a minor difference between the top and bridge sites, and we therefore only show the DOS of the top and hollow sites. As shown in Fig. 4, the
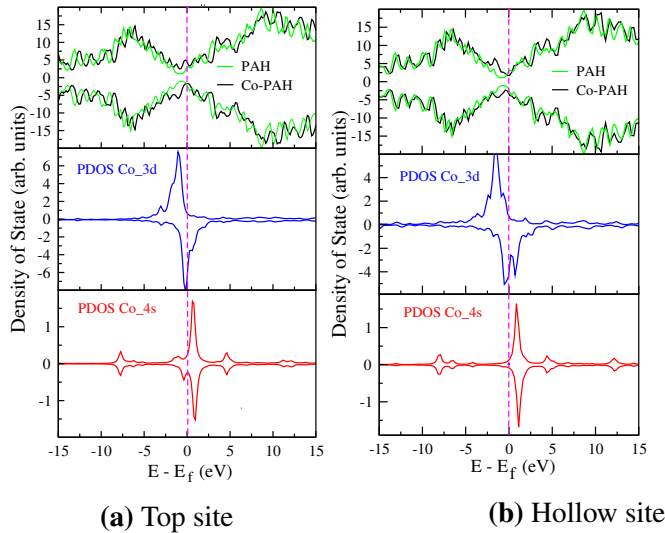

(a) Top site

(b) Hollow site

Figure 4 Total Density of state (TDOS) and partial density of state (PDOS) of the Co-PAH complex for different adsorption sites. The majority spin (spin up) and minority spin (spin down) of TDOS of the PAH molecule and the Co-PAH complex at the top (a), and the hollow (b) sites are illustrated. The PDOS of the Co_{3d} and the Co_{4s} states are also shown.

electronic structure of the PAH surface is perturbed by adsorption of the Co atom. The Fermi level (E_f) of the PAH surface is shifted upward by 0.50, 0.47

and 0.21 eV for the top, bridge and hollow sites, respectively, which is due to electron transfer from the Co adatom to the PAH surface. The analysis of the PDOS clearly indicates that the DOS distributes symmetrically for both majority and minority spins of the 4s states of the Co atom, resulting a zero net magnetic moment from these configuration. The unequal distribution of the majority and minority spins of the d orbitals of the Co atom at the Fermi level is the origin of the spin polarization and magnetic moment in the Co-PAH complex. The 4s states of the Co atom is located above E_f in both majority and minority spins for the hollow site and do not show a significant contribution to the occupied states, indicating a larger promotion of 4s electrons into the 3d states of the Co atoms and also the decrease of the magnetic moment of the Co atom. While for the top and bridge sites there are small contributions from both majority and minority spins of the 4s state into the occupied orbitals. The unfilled states above the Fermi level are the source of free carriers, which are responsible for most of the electron transport around the Fermi level.[155] According to Fig. 4, the majority spin of the 3d states lies completely below E_f for all three adsorption sites, while the minority spins are at E_f for both top and bridge (a bit shifted upward) sites, and for the hollow site it splitted into two peaks above and below E_f.

The orbital occupation of the Co atom based on the Mulliken population analysis shows that 1.4 electrons are transferred from the 4s orbitals to the 3d orbitals, and 0.2 electrons also transferred from the 4s orbitals of the Co atom to the π orbitals of the PAH surface, according to the charge transfer analysis. But the net magnetic moment is reduced from 3.0 μ_B in the isolated Co atom to 1.07 μ_B in the Co adatom on the hollow site. The depletion of net magnetic moment, 1.93 μ_B, suggest that the Co adsorption induces a magnetic moment to the PAH surface which is opposite to the moment of the adatom, and reduces the overall magnetic moment in the Co-PAH system. This is clearly visible from the PDOS analysis of the 2p states of the carbon

atoms in the hexagonal ring in contact with the Co adatom (see Fig. 5).
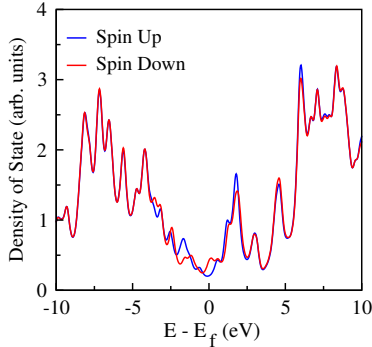
Furthermore, to investigate the effects of spin mul-

Figure 5 Partial density of state of the $2p$ states of the carbon atoms in the hexagonal ring in contact with the Co adatom in the hollow site.

tiplicity on the electronic properties of the Co-PAH complex, we analyzed the density of states obtained for the doublet and quartet states, for the hollow configuration, Fig. 6. Fig. 6b, shows that the minority spin of the $3d$ states of the Co atom at the hollow site is shifted above E_f, on the other hand the majority spin of the $4s$ state is located at the Fermi level and takes considerable contributions to the occupied states and participates in the spin polarization. Therefore, the hybridization between the localized $3d$ orbital of the Co atom and the π orbitals of the PAH surface is suppressed due to the Pauli repulsion between the π orbitals and the diffuse $4s$ states, which is the origin of the reduction of the adsorption energy by 1 eV from the doublet state to the quartet state.

Chemisorption or Physisorption?

The adsorption energy gives us a direct indication of the type (chemisorbed or physisorbed) of the metal-graphene interaction. There have been a numerous theoretical studies that focused on the Co/graphene interaction and they predict a relatively large adsorption energy, resulting from strong hy-
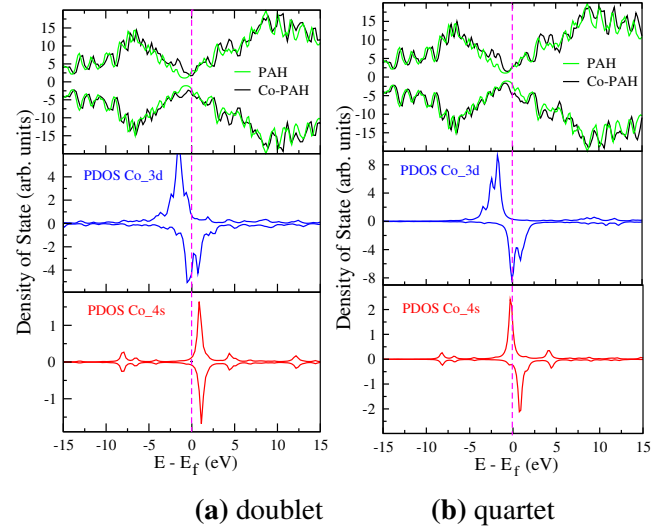

(a) doublet   **(b)** quartet

Figure 6 Total Density of state (TDOS) and partial density of state (PDOS) of the Co-PAH complex for the different spin states. The majority spin (spin up) and minority spin (spin down) of TDOS of the PAH molecule and the Co-PAH complex at the hollow site for the doublet (a) and the quartet (b) states are illustrated. The PDOS of the individual contribution from the Co_{3d} and the Co_{4s} states are also shown.

bridization between the cobalt $3d$- and graphene π-orbitals.[13,152,156–159] Rudenko *et al.*[78] used a multi-configurational CASSCF formalism to reproduce the potential energy curves for different electronic configurations of the Co atom approaching the graphene surface. They found two binding mechanisms for these interactions. The first corresponds to a physisorption of the Co adatom in the high-spin $3d^7 4s^2$ configuration (at the equilibrium distance of 3.1 Å), and the second results from the chemical bonding formed by strong orbital hybridization in the low-spin $3d^9 4s^0$ state (at the equilibrium distance of 1.6 Å). Our calculated adsorption energy and also the DOS analysis predict a chemisorbed interaction between the Co adatom and the PAH surface at the equilibrium distance of 1.65 Å, which is consistent with these potential energy curves. While a typical binding energy of a physisorption is small (50−200 meV) and a binding energy of more than 500 meV is considered as a
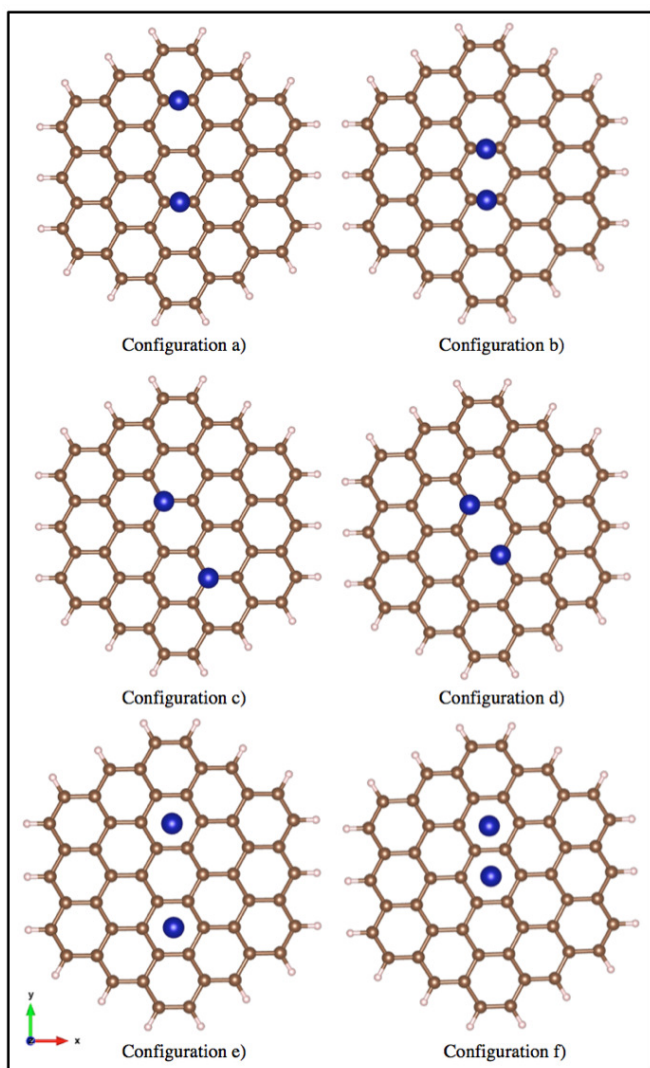
Figure 7 Stable configurations for the parallel adsorption of the Co dimer and two separate Co atoms on the $C_{54}H_{18}$ molecule. Blue, brown and pink circles indicate Co, C, and H atoms, respectively. The configurations *a* and *b* are the bridge sites, *c* and *d* are the top sites, and *e* and *f* are the hollow sites, respectively.

chemisorption,[79] the Co-graphene interaction with an adsorption energy of 970 meV has been considered as a physisorbed interaction.[10]

From the experimental side, the layer-spacing between the graphene sheets and metal surfaces would be an important resource for a better understanding of these interactions. For the metal-graphene, spacing values between approximately 2.1 and 3.8 Å

have been found, depending on the metal,[160] and if a graphene sheet is physisorbed on a metal surface, one would expect a distance comparable to the layer spacing of 3.35 Å in bulk graphite.[160] An STM measurement reported a spacing of 1.5−2.2 Å between the graphene film and the Co(0001) surface,[161] indicating a strong interaction between the Co/graphene interface layer. In the case of the adatom adsorption, one can measure the island density upon the metal adsorption and get more information about the diffusion of the adatom on the graphene surface using STM experiment. According to the classical theory of nucleation, for fast diffusion the island density is low and for slow diffusion the island density is high.[162] The activation energy for in-plane migration of the Au and Pt atoms on the graphene sheet (at 600 °C) is measured around 2.5 eV using transmission electron microscopy studies,[163] indicating covalent bonding between the metal and carbon atoms. While Johll *et al.*[10] suggested a physisorbed interaction between the Fe adatom and the graphene surface, Liu *et al.*[159] measured a high island density of 4.3×10^3 islands/$Å^2$ for the Fe deposited on the graphene at room temperature, indicating a high diffusion barrier.

Co dimer on the PAH surface

For adsorption of the Co dimer on the PAH surface, there are also several possibilities and initially, as for the Co-PAH system, we looked at many more adsorption configurations, but we only present six configurations as representative for the bridge, top and the hollow sites, including both parallel and perpendicular configurations of the dimers on the PAH surface. The distortion of the PAH molecule and the Co dimer upon adsorption at the parallel configuration and at different adsorption sites are shown in Fig. 7. For adsorption of the Co dimer on the PAH surface, as for the Co-PAH complex, we also did a constraint optimization to find the adsorption energy of the Co dimer on the highly

Table 5 Results for the parallel Co dimer adsorbed on the $C_{54}H_{18}$ molecule with configurations according to Fig. 7 for different spin multiplicities (2S+1). The adsorption energy (E_{ads}), interfacial interaction energy (E_{int}), Co-Co distance (d_{Co-Co}), Co-C distance (d_{Co-C}, distance between the Co atom and nearest carbon atoms), adsorption height (h) of the Co atom with respect to the averaged z coordinates of the C atoms in the PAH molecule, magnetic moment on each Co atom (M), the Hirshfeld atomic charge and the $<S^2>$ values are given.

Configuration	2S+1	E_{ads} (eV)	E_{int} (eV)	d_{Co-Co} (Å)	d_{Co-C} (Å)	h (Å)	M (μ_B/atom)	Charge (e)	$<S^2>$
Config. a)	3	-1.15	—	4.87	1.93	1.82	1.16, 1.15	0.21, 0.22	2.10
	5	-1.04	—	4.87	1.94	1.83	1.92, 1.89	0.16, 0.17	6.14
	7	-0.85	—	4.87	2.18	1.96	2.97, 2.97	0.12, 0.12	12.11
Config. b)	3	-2.41	-0.07	2.44	1.95	1.80	1.08 ,1.08	0.14, 0.14	2.11
	5	-2.76	-0.34	2.44	2.01	1.94	2.14, 2.14	0.09, 0.09	6.12
	7	-2.07	0.34	2.44	2.06	2.02	2.41, 2.41	0.18, 0.18	12.08
Config. c)	3	-0.98	—	4.22	1.88	1.94	1.18, 1.18	0.13, 0.13	2.09
	5	-0.84	—	2.22	1.90	1.95	1.86, 1.82	0.07, 0.08	6.12
	7	-0.51	—	4.22	2.09	2.12	2.96, 2.96	0.16, 0.16	12.08
Config. d)	3	-2.01	0.40	2.81	1.93	1.96	1.04, 1.04	0.15, 0.15	2.09
	5	-2.23	0.17	2.81	1.99	2.05	2.07, 2.07	0.11, 0.11	6.10
	7	-1.47	0.93	2.81	2.06	2.15	2.57, 2.57	0.19, 0.19	12.05
Config. e)	3	-2.21	—	4.78	1.96	1.47	1.14, 1.08	0.18, 0.24	2.09
	5	-1.79	—	4.78	2.06	1.48	1.91, 1.86	0.16, 0.19	6.12
	7	-0.98	—	4.78	2.08	1.51	2.85, 2.76	0.16, 0.19	12.09
Config. f)	3	-2.78	-0.37	2.35	2.04	1.49	1.04, 1.08	0.18, 0.16	2.08
	5	-2.94	-0.53	2.35	2.08	1.51	2.09, 2.08	0.08, 0.08	6.10
	7	-2.03	0.37	2.35	2.10	1.52	2.76, 2.73	0.14, 0.15	12.06

symmetric adsorption sites. After a complete relaxation of geometry, the Co dimer moves away from the top and bridge sites, which is consistent with the results from the Co-PAH complex. Furthermore, we also calculated the vibrational frequencies for the stationary points. For the hollow configuration, no imaginary frequency is observed indicating it is a stable minimum on the potential energy surface. But for the bridge and top configurations, a single imaginary frequency of -101.76 and -66.21 cm^{-1}, respectively, showing that they are not minima on the potential energy surface.

All structural, electronic and magnetic properties of the parallel Co dimers on the PAH surface, for different spin multiplicities (2S+1), are given in Table 5. The adsorption energies for the ground state of the parallel Co dimers adsorbed on two neighbouring bridge (Fig. 7b), top (Fig. 7d) and hollow (Fig. 7f) sites of the PAH surface are found to be -2.76 and -2.23 and -2.94 eV, respectively. These values are significantly more attractive than the adsorption energies of two separated Co atoms on the bridge (Fig. 7a), top (Fig. 7c) and hollow (Fig. 7e) sites of the PAH surface, by -1.15, -0.98 and -2.21 eV, respectively, indicating that aggregation of the Co atoms on the PAH surface is favorable, in agreement with observations by STM.[164] Comparing the three adsorption sites, we can conclude that the hollow site is the favorable adsorption site for the parallel Co dimer, as compared to the bridge and top sites. The Co-C bond distance increases with the coordination of the Co atom, from the top over

Table 6 Results for the perpendicular Co dimer adsorbed on the $C_{54}H_{18}$ molecule with configurations according to Fig. 8 for different spin multiplicities (2S+1). The adsorption energy (E_{ads}), interfacial interaction energy (E_{int}), Co-Co distance (d_{Co-Co}), Co-C distance (d_{Co-C}, the distance between the Co atom and nearest carbon atoms), adsorption height (h) of the Co atom in contact with the PAH surface (Co^1) with respect to the averaged z coordinates of the C atoms in the PAH molecule, magnetic moment on each Co atom (M), the Hirshfeld atomic charge and the $< S^2 >$ values are given. The values in parentheses are related to the Co atom further from the PAH surface (Co^2).

Configuration	2S+1	E_{ads} (eV)	E_{int} (eV)	d_{Co-Co} (Å)	d_{Co-C} (Å)	h (Å)	M (μ_B/atom)	Charge (e)	$< S^2 >$
Config. a)	3	-2.78	-0.37	2.16	2.11	2.01	-0.58 (2.54)	0.09 (0.06)	2.11
	5	-3.40	-0.99	2.07	2.11	2.08	1.89 (2.35)	0.08 (0.02)	6.08
	7	-2.51	-0.10	2.03	2.15	2.10	2.24 (2.45)	0.18 (0.13)	12.05
Config. b)	3	-2.48	-0.02	2.12	2.09	2.20	0.14 (2.03)	0.09 (-0.04)	2.12
	5	-3.32	-0.91	2.02	2.09	2.18	1.89 (2.34)	0.08 (0.00)	6.10
	7	-2.43	-0.07	2.02	2.12	2.22	2.26 (2.46)	0.18 (0.13)	12.05
Config. c)	3	-3.21	-0.80	2.19	2.10	1.52	-0.39 (2.42)	0.04 (0.01)	2.10
	5	-3.92	-1.51	2.06	2.14	1.55	1.49 (2.51)	0.03 (0.01)	6.09
	7	-2.68	-0.30	2.03	2.30	1.63	2.18 (2.49)	0.14 (0.12)	12.05

bridge to the hollow sites.

In addition, we also placed the Co dimer in a perpendicular configuration to the PAH surface on the three adsorption sites, and optimized the structures (see Fig. 8), and the results are given in Table 6. According to the frequency analysis, the hollow site is here also found to be a stable minimum on the potential energy surface whereas the bridge and top configurations, with the frequencies of -104.76 and -88.53 cm^{-1}, respectively, are not minima on the potential energy surface. After a complete relaxation they move toward the hollow site and stay perpendicular to the PAH surface.

The adsorption energies for the ground state of the perpendicular Co dimer on the bridge, top and the hollow sites of the PAH surface are found to be -3.40 and -3.32 and -3.92 eV, respectively, indicating that the hollow site is also here the most favorable adsorption site (see Table 6). For the perpendicular configuration, the Co-C bond length for the top, bridge and hollow sites are found to be 2.09, 2.11 and 2.14 Å, respectively, which also increases slightly with the coordination of the Co atom. The Co-Co bond length of 2.02, 2.07 and 2.06 Å for the top, bridge and the hollow sites, respectively,

represent a small deviation from the bond length of the free dimer, which is calculated to 1.96 Å for the ground state.

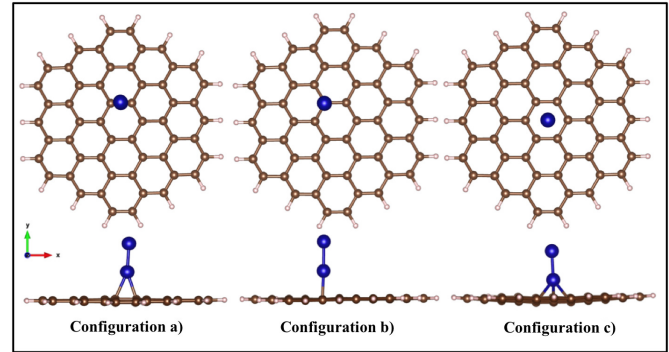From the adsorption energies, E_{ads} in the Tables 5

Figure 8 Stable configurations for the perpendicular Co dimer adsorbed on the $C_{54}H_{18}$ molecule. Blue, brown and pink circles indicate Co, C, and H atoms, respectively. *a*, *b* and *c* configurations are the bridge, top and hollow sites, respectively.

and 6, we conclude that the adsorption of the perpendicular Co dimer is more stable than the parallel dimer. This is in agreement with previous theoretical calculations.[117,118] The adsorption energy

has two important contributions, the Co-Co interaction energy and the interaction energy between the dimer and the surface. For example, the perpendicular Co dimer at the hollow site (Fig. 7c), has the adsorption energy of -3.92 eV for the ground electronic state (see Table 6). This value should be compared to the sum of the binding energy of the free dimer, -2.42 eV, and the adsorption energy for two isolated Co atoms on the PAH surface, where the adsorption energy for the isolated Co atom on the hollow site is -1.04 eV. The binding energy of the dimer with the PAH surface is significantly lower than the value expected simply from the sum of the binding energy of the isolated adatoms. The reason of this reduction is a weaker dimer bond on the surface and a weaker Co_2-PAH interaction compared to the isolated adatom interactions, which is due to rehybridization effects.[165] In that work,[165] it was shown that the presence of a neighbouring Al atom weakens the Al-substrate bond and also the presence of the substrate weakens the Al-Al bond, because the valence electrons involved in the dimer bond relocate and participate in the Al-substrate bond. Therefore binding of a single Co atom to the surface is stronger than binding of a Co dimer to the surface. Hence the Co-C bond length in the Co-PAH complex is mostly shorter than the corresponding bond length in the Co_2-PAH complex.

The interfacial interaction energy, E_{int}, which measures the interaction energy of the Co dimer with the PAH surface is also given in Tables 5 and 6. E_{int} for the perpendicular configuration is more attractive than for the parallel configuration, due to the energy penalty resulted from the Co-Co bond elongation in the parallel configurations. Therefore, the perpendicular adsorbed Co dimer on the PAH surface is more stable than the parallel Co dimer.

In contrast to the Co-PAH system, the interaction of the Co dimer with the PAH surface is not accompanied by a change in the spin state, and the most stable spin state is still the quintet state. This confirms that the Co-C interaction is weaker than the Co-Co interaction. For two separate Co atom on the

PAH surface (see Fig. 7 and Table 5), the triplet state is found to be the most stable state, which means each Co atom has one unpaired electron as for the Co adatom on the PAH surface, where the doublet state was the most stable spin state. The small deviation of the expectation value $< S^2 >$ from the ideal value, as seen in Tables 5 and 6, confirm again the good performance of the S12g functional for calculating the spin states of transition metal complexes. The Hirshfeld charge analysis[98] shows also a positive charge for the Co dimer on the PAH surface, but the magnitude of the charge transfer between the Co dimer and the PAH surface is smaller than the amount of the charge transfer from the Co adatom to the PAH surface (see Tables 4, 5 and 6). It is found that for the perpendicular Co dimer, Fig. 8, the Co atom in contact with the PAH surface lose more partial electronic charge than the Co atom further from the PAH surface and form an electric dipole moment. However, for the parallel Co dimer, Fig. 7, the Co atoms lose almost the same amount of electrons.

We also calculated the projected magnetic moment of each Co atom in the Co_2-PAH complex at different adsorption sites and different configurations. As for the adsorbed Co adatom on the PAH surface, the projected magnetic moment of the two separated Co atoms are also reduced upon adsorption and the amount of reduction is dependent on the adsorption site. This is actually expected because the charge transfer that occurs between the Co adatoms and the PAH surface and also the promotion of electrons from $4s$ to $3d$ states of the Co atoms during the adsorption, change the populations of the d and s orbitals of the adatoms. But for the adsorption of the Co dimer, the spin state and the projected electronic configuration on the Co atoms retain the characteristics of the free Co dimer. Therefore the net amount of the charge transfer from the Co dimer to the PAH surface is small and also the total magnetic moment of the Co_2-PAH complex, which is mainly localized on the Co atoms, is almost retained upon adsorption. For the perpendicular Co dimer, the projected magnetic moment on the Co atom further from the
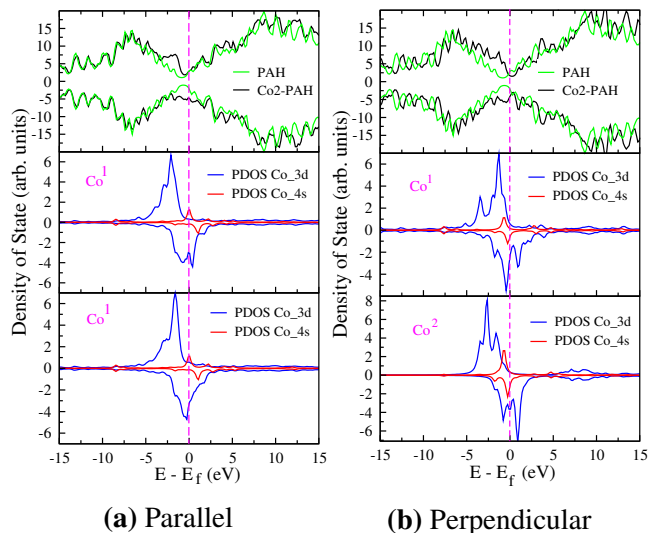
Figure 9 Total Density of state (TDOS) and partial density of state (PDOS) of the Co_2-PAH complex for the parallel (a) and perpendicular (b) configurations at the hollow site. The majority spin (spin up) and minority spin (spin down) of the TDOS of the PAH molecule and the Co_2-PAH complex are illustrated. The PDOS of the individual contribution from the Co_{3d} and the Co_{4s} states are also shown. The Co^1 and Co^2 refer to the Co atom in contact and further from the PAH surface, respectively. In the parallel configuration, both Co atoms are in contact with the PAH surface, Co^1.

PAH surface (Co^2) is increased with respect to the Co atoms in the free dimer, but for the Co atom in contact with the PAH surface (Co^1), the projected magnetic moment is reduced in respect to the corresponding value of the Co atoms in the free dimer. Figs. 9a and 9b show the DOS of the Co dimer adsorbed on the hollow site of the PAH surface for the parallel and perpendicular configurations, respectively, together with the individual contributions from the 3d and 4s states of the Co atoms. Both the majority and minority spin of the PAH surface are significantly modified around the Fermi level, demonstrating a change in the electronic structure of the PAH surface upon adsorption of the Co dimer. The Fermi level of the PAH surface is shifted upward by 0.7 and 0.5 eV for the parallel and perpendicular

dimer, respectively, indicating charge transfer from the Co dimer to the PAH surface. Fig. 9, clearly shows that both the majority and minority spin of the 3d and 4s of the Co dimer are responsible for magnetism in the Co_2-PAH complex. For the parallel Co dimer, the majority spin of the 4s states of the Co atoms are located at the Fermi level and the minority spins are shifted above E_f. However, for the perpendicular dimer, both the majority and minority spins of the 4s states of the Co atoms are below the Fermi level and participating in the hybridization with the Co_{3d} and C_{2p} states, resulting in stronger hybridization and increasing the adsorption energy by 0.98 eV more than the parallel configuration. The majority and minority spins of the 3d states of the Co atoms in the perpendicular adsorption are split into two peaks, which the majority spins are spanning below the E_f and the minority spins are spanning at Fermi level. For the Co atom further from the PAH surface, the minority spin of the 3d states are moved further up from E_f and have less contribution to the occupied states than the minority spin of the 3d states of the Co atom closer to the PAH surface. This is the origin of the difference in the magnetic moment of the Co atoms in the perpendicular dimer on the PAH surface, which comes from the antiferromagnetic coupling of the Co atoms in this configuration. The bonding character from DOS analysis agrees well with the results from adsorption energy and suggest a strong chemisorption of the Co atom and dimer on the PAH surface.

Therefore, the Co adatoms interact with the PAH surface, resulting in a modification in the electronic properties of the Co adatoms and it is well known that the catalytic activity of the metal particles strongly depends on their electronic properties.[166] Our results also show a charge transfer from the Co adatoms to the PAH surface and suggest that modifying the conditions for charge transfer from the Co adatoms to the PAH support may yield significant changes in catalytic behavior.

Conclusions

A detailed density functional study of the Co adatom and dimer adsorbed on a PAH surface is presented. The nature of the interaction between the Co atom and dimer with the PAH surface is elucidated. The results are analyzed in terms of structural, electronic and magnetic properties. It was shown that the circumcoronene molecule can successfully use as the model for representing the graphene surface in this study. The adsorption energy indicates that the Co adatom adsorb on the hollow site of the PAH. Due to rehybridization effects, binding of the single Co atom to the surface is stronger than binding of the Co dimer to the PAH surface. A small charge transfer takes place from the Co atom and dimer to the PAH surface giving a positive charge on the Co adatoms, which modifies the catalytic activity. In general the modification of the atomic charges by the binding of metal particles to a carbon-supported material can be used to tune the catalytic properties of the metal particles. The bonding character of the Co atom and dimer adsorbed on the PAH have a covalent component, arising from strong hybridization between the d orbitals of the Co adatoms and p_z orbitals of the surface-carbon atoms. Upon adsorption, the magnetic moment of the Co atom is reduced depending on the adsorption sites and adsorption configurations. The total reduction of net magnetic moment suggests that the Co adsorption induces a magnetic moment to the PAH surface which is opposite to the moment of the adatom and reduces the overall magnetic moment in the Co-PAH complex. Density of state analysis shows a promotion of electrons from $4s$ states to the $3d$ states of Co adatom upon adsorption, which is the main contribution of the magnetic moment reduction. For the perpendicular Co dimer, the projected magnetic moment on the Co atom further from the PAH is increased, due to the antiferromagnetic coupling between Co atoms in this configuration. These results provide insight into the modification of the PAH surface to enhance its bonding with the Co atom and dimer, which may be a guide for experimental groups that are considering the use of atoms and molecules as building blocks for designing a new metal-carbon nanostructures and carbon-based catalysts.

References

(1) Novoselov, K. S.; Geim, A. K.; Morozov, S. V.; Jiang, D.; Zhang, Y.; Dubonos, S. V.; Grigorieva, I. V.; Firsov, A. A. *Science* **2004**, *306*, 666–669.

(2) Geim, A. K.; Novoselov, K. S. *Nature Mater.* **2007**, *6*, 183–191.

(3) Katsnelson, M. I. *Mat. Today* **2007**, *10*, 20–27.

(4) El-Kady, M. F.; Strong, V.; Dubin, S.; Kaner, R. *Science* **2012**, *335*, 1326–1330.

(5) Dresselhaus, M. S.; Dresselhaus, G. *Adv. Phys.* **1981**, *30*, 139–326.

(6) Kelly, B. T. *Physics of Graphite*; Applied Science: London, 1981.

(7) Wang, X.; Zhi, L.; Müllen, K. *Nano Lett.* **2008**, *8*, 323–327.

(8) Geim, A. K. *Science* **2009**, *324*, 1530–1534.

(9) Yagi, Y.; Briere, T. M.; Sluiter, M. H. F.; Kumar, V.; Farajian, A. A.; Kawazoe, Y. *Phys. Rev. B* **2004**, *69*, 075414–9.

(10) Johll, H.; Kang, H. C. *Phys. Rev. B* **2009**, *79*, 245416–18.

(11) Chan, K. T.; Neaton, J. B.; Cohen, M. L. *Phys. Rev. B* **2008**, *77*, 235430–12.

(12) Giovannetti, G.; Khomyakov, P. A.; Brocks, G.; Karpan, V. M.; Brink, J. V. D.; Kelly, P. J. *Phys. Rev. Lett.* **2008**, *101*, 026803–4.

(13) Cao, C.; Wu, M.; Jiang, J. Z.; Cheng, H. P. *Phys. Rev. B* **2010**, *81*, 205424–9.

(14) Sevinçli, H.; Topsaka, M.; Durgun, E.; Ciraci, S. *Phys. Rev. B* **2008**, *77*, 195434–7.

(15) Uchoa, B.; Lin, C.-Y.; Castro-Neto, A. H. *Phys. Rev. B* **2008**, *77*, 035420–5.

(16) Okamoto, Y. *Chem. Phys. Lett.* **2006**, *420*, 382–386.

(17) Okazaki-Maeda, K.; Yamakawa, S.; Morikawa, Y.; Akita, T.; Tanaka, S.; Hyodo, S.; Kohyama, M. *J. Phys.: Conf. Ser.* **2008**, *100*, 072044–4.

(18) Shylesh, S.; Schüneman, V.; Thiel, W. R. *Angew. Chem. Int. Ed.* **2010**, *49*, 3428–3459.

(19) Narayanan, R.; El-Sayed, M. A. *Nano Lett.* **2004**, *4*, 1343–1348.

(20) Prado-Burguete, C.; Linares-Solano, A.; Rodriguez-Reinoso, F.; de Lecea, C.-M. *J. Catal.* **1991**, *128*, 397–404.

(21) Chen, M.; Goodman, D. *Catal. Today* **2006**, *111*, 22–33.

(22) van Leeuwen, D. A.; van Ruitenbeek, J. M.; de Jongh, L. J. *Phys. Rev. Lett.* **1994**, *73*, 1432–1435.

(23) Chekulaev, M. S.; Kozyrev, S. V.; Ivanov-Omskii, V. I.; Yastrebov, S. G.; Zvonareva, T. K.; Siklitskaya, A. V. *J. Phys.: Conf. Ser.* **2014**, *572*, 012024–5.

(24) Gruner, M. E.; Rollmann, G.; Hucht, A.; Entel, P. In *Advances in Solid State Physics*; Haug, P. D. R., Ed.; Springer Berlin Heidelberg, 2008; Vol. 47; Chapter III, pp 117–128.

(25) Bobadova-Parvanova, P.; Jackson, K. A.; Srinivas, S.; Horoi, M. *J. Chem. Phys.* **2005**, *122*, 014310–11.

(26) Wang, S.-Y.; Yu, J.-Z.; Mizuseki, H.; Yan, J.-A.; Kawazoe, Y.; Wang, C.-Y. *J. Chem. Phys.* **2004**, *120*, 8463–8468.

(27) Payne, F. W.; Jiang, W.; Bloomfield, L. A. *Phys. Rev. Lett.* **2006**, *97*, 193401–4.

(28) Šipr, O.; Košuth, M.; Ebert, H. *Phys. Rev. B* **2004**, *70*, 174423–13.

(29) Tiago, M. L.; Zhou, Y.; Alemany, M. M. G.; Saad, Y.; Chelikowsky, J. R. *Phys. Rev. Lett.* **2006**, *97*, 147201–4.

(30) Baletto, F.; Ferrando, R. *Rev. Mod. Phys.* **2005**, *77*, 371–423.

(31) Douglass, D. C.; Cox, A. J.; Bucher, J. P.; Bloomfield, L. A. *Phys. Rev. B* **1993**, *47*, 12874–12889.

(32) Billas, I. M. L.; Châtelain, A.; de Heer, W. A. *Phys. Rev. B* **1997**, *168*, 64–84.

(33) Gerion, D.; Hirt, A.; Billas, I. M. L.; Châtelain, A.; de Heer, W. A. *Phys. Rev. B* **2000**, *62*, 7491–7501.

(34) Xu, X.; Yin, S.; Moro, R.; de Heer, W. A. *Phys. Rev. Lett.* **2005**, *95*, 237209–4.

(35) Dong, C. D.; Gong, X. G. *Phys. Rev. B* **2008**, *78*, 020409–4.

(36) Dry, M. E. *J. Chem. Technol. Biotechnol.* **2002**, *77*, 43–50.

(37) Khodakov, A. Y.; Chu, W.; Fongarland, P. *Chem. Rev.* **2007**, *107*, 1692–1744.

(38) Dìaz, J. A.; Akhavan, H.; Romero, A.; Garcia-Minguillan, A. M.; Romero, R.; Giroir-Fendler, A.; Valverde, J. L. *Fuel Process. Technol.* **2014**, *128*, 417–424.

(39) Bezemer, G. L.; van laak, A.; van Dillen, A. J.; de Jong, K. P. *J. Solid State Chem.* **2004**, *147*, 259–264.

(40) Tavasoli, A.; Sadagiani, K.; Khorashe, F.; Seifkordi, A. A.; Rohani, A. A.; Nakhaeipour, A. *Fuel Process. Technol.* **2008**, *89*, 491–498.

(41) Guo, S.; Zhang, S.; Wu, L.; Sun, S. *Angew. Chem. Int. Ed.* **2012**, *51*, 11770–11773.

(42) Mahmoodinia, M.; Ebadi, M.; Åstrand, P.-O.; Chen, D.; Cheng, H.-Y.; Zhu, Y.-A. *Phys. Chem. Chem. Phys.* **2014**, *16*, 18586–18595.

(43) Karpan, V. M.; Khomyakov, P. A.; Starikov, A. A.; Giovannetti, G.; Zwierzycki, M.; Talanana, M.; Brocks, G.; van den Brink, J.; Kelly, P. J. *Phys. Rev. B* **2008**, *78*, 195419–11.

(44) Sanz-Navarro, C. F.; Åstrand, P.-O.; Chen, D.; Rønning, M.; van Duin, A. C. T.; Jacob, T.; Goddard, W. A. *J. Phys. Chem. A* **2008**, *112*, 1392–1402.

(45) Cheng, H.-Y.; Zhu, Y.-A.; Åstrand, P.-O.; Chen, D.; Li, P.; Zhou, X.-G. *J. Phys. Chem. C* **2013**, *117*, 14261–14271.

(46) Fampiou, I.; Ramasubramanian, A. *J. Phys. Chem. C* **2012**, *116*, 6543–6555.

(47) Duffy, D. M.; Blackman, J. A. *Phys. Rev. B* **1998**, *58*, 7443–7449.

(48) Müller, U.; Sattler, K.; Xhie, J.; Venkateswaran, N.; Raina, G. *J. Vac. Sci. Technol. B* **1991**, *9*, 829–832.

(49) Müller, U.; Sattler, K.; Xhie, J.; Venkateswaran, N.; Raina, G. *Z. Phys. D: At. Mol. Clusters* **1991**, *19*, 319–321.

(50) Liu, L.; Su, Y.; Gao, J.; Zhao, J. *Physica E* **2012**, *46*, 6–11.

(51) Santos, E. J. G.; Sánchez-Portal, D.; Ayuela, A. *Phys. Rev. B* **2010**, *81*, 125433–6.

(52) Wang, Z.; Xiao, J.; Li, M. *Appl. Phys. A* **2013**, *110*, 235–239.

(53) Virgus, Y.; Purwanto, W.; Krakauer, H.; Zhang, S. *Phys. Rev. B* **2012**, *86*, 241406–5.

(54) Frelink, T.; Visscher, W.; Veen, J. V. *J. Electroanal. Chem.* **1995**, *382*, 65–72.

(55) Lee, S. A.; Park, K. W.; Choi, J. H.; Kwon, B. K.; Sung, Y. E. *J. Electrochem. Soc.* **2002**, *149*, 1299–1304.

(56) Mukerjee, S.; McBreen, J. *J. Electroanal. Chem.* **1998**, *448*, 163–171.

(57) Park, S.; Wasileski, S. A.; Weaver, M. J. *J. Phys. Chem. B* **2001**, *105*, 9719–9725.

(58) Jiménez-Halla, J. O. C.; Robles, J.; Solà, M. *J. Phys. Chem. A* **2008**, *112*, 1202–1213.

(59) Cheng, H.-Y.; Åstrand, P.-O.; Chen, D.; Zhu, Y.-A.; Zhou, X.-G.; Li, P. *Chem. Phys. Lett.* **2013**, *575*, 76–80.

(60) Rigo, V. A.; Martins, T. B.; da Silva, A. J. R.; Fazzio, A.; Miwa, R. H. *Phys. Rev. B* **2009**, *79*, 075435–9.

(61) Sony, P.; Puschnig, P.; Nabok, D.; Ambrosch-Draxl, C. *Phys. Rev. Lett.* **2007**, *99*, 176401–4.

(62) Atodiresei, N.; Caciuc, V.; Lazić, P.; Blügel, S. *Phys. Rev. Lett.* **2009**, *102*, 136809–4.

(63) Mura, M.; Gulans, A.; Thonhauserc, T.; Kantorovich, L. *Phys. Chem. Chem. Phys.* **2010**, *12*, 4759–4767.

(64) Brede, J.; Atodiresei, N.; Kuck, S.; Lazić, P.; Caciuc, V.; Morikawa, Y.; Hoffmann, G.; Blüge, S.; Wiesendanger, R. *Phys. Rev. Lett.* **2010**, *105*, 047204–4.

(65) Mercurio, G.; McNellis, E. R.; Martin, I.; Hagen, S.; Leyssner, F.; Soubatch, S.; Meyer, J.; Wolf, M.; Tegeder, P.; Tautz, F. S.; Reuter, K. *Phys. Rev. Lett.* **2010**, *104*, 036102–4.

(66) Stradi, D.; Barja, S.; Diaz, C.; Garnica, M.; Borca, B.; Hinarejos, J. J.; Sánchez-Portal, D.; Alcami, M.; Arnau, A.; de Parga, A. L. V.; Miranda, R.; Martin, F. *Phys. Rev. Lett.* **2011**, *106*, 186102–4.

(67) Grimme, S. *J. Comput. Chem.* **2004**, *25*, 1463–1473.

(68) Grimme, S. *J. Comput. Chem.* **2006**, *27*, 1787–1799.

(69) Bloński, P.; Hafner, J. *J. Chem. Phys.* **2012**, *136*, 074701–11.

(70) Cramer, C. J.; Truhlar, D. G. *Phys. Chem. Chem. Phys.* **2009**, *11*, 10757–10816.

(71) Dyall, K. G.; Faegri, K. *Introduction to Relativistic Quantum Chemistry*; Oxford University Press: New York, USA, 2007.

(72) van Lenthe, E.; Ehlers, A.; Baerends, E. *J. Chem. Phys.* **1999**, *110*, 8943–8953.

(73) van Lenthe, E.; Baerends, E. J.; Snijders, J. G. *J. Chem. Phys.* **1993**, *99*, 4597–4610.

(74) van Lenthe, E.; Baerends, E. J.; Snijders, J. G. *J. Chem. Phys.* **1994**, *101*, 9783–9792.

(75) van Lenthe, E.; Snijders, J.; Baerends, E. *J. Chem. Phys.* **1996**, *105*, 6505–6516.

(76) van Lenthe, E.; van Leeuwen, R.; Baerends, E. J.; Snijders, J. G. *Int. J. Quant. Chem.* **1996**, *57*, 281–293.

(77) Heully, J. L.; Lindgren, I.; Lindroth, E.; Lundqvist, S.; Martensson-Pendrill, A. M. *J. Phys. B: At. Mol. Phys.* **1986**, *19*, 2799–2815.

(78) Rudenko, A. N.; Keil, F. J.; Katsnelson, M. I.; Lichtenstein, A. I. *Phys. Rev. B* **2012**, *86*, 075422–11.

(79) Voloshina, E.; Usvyat, D.; Schütz, M.; Dedkov, Y.; Paulus, B. *Phys. Chem. Chem. Phys.* **2011**, *13*, 12041–12047.

(80) Kandalam, A. K.; Kiran, B.; Jena, P.; Li, X.; Grubisic, A.; Bowen, K. H. *J. Chem. Phys.* **2007**, *126*, 084306–9.

(81) Velde, G. T.; Bickelhaupt, F. M.; Baerends, E. J.; Guerra, C. F.; van Gisbergen, S. J. A.; Snijders, J. G.; Ziegler, T. *J. Comput. Chem.* **2001**, *22*, 931–967.

(82) Guerra, C. F.; Snijders, J. G.; Velde, G. T.; Baerends, E. J. *Theor. Chem. Acc.* **1998**, *99*, 391–403.

(83) Swart, M. *Chem. Phys. Lett.* **2013**, *580*, 166–171.

(84) Swart, M.; Solà, M.; Bickelhaupt, F. M. *J. Comput. Meth. Sci. Engin.* **2009**, *9*, 69–77.

(85) Swart, M.; Solà, M.; Bickelhaupt, F. M. *J. Chem. Phys.* **2009**, *131*, 094103–9.

(86) Grimme, S. *WIREs Comput. Mol. Sci.* **2011**, *1*, 211–228.

(87) Gruden-Pavlović, M.; Stepanović, S.; Perić, M.; Güell, M.; Swart, M. *Phys. Chem. Chem. Phys.* **2014**, *16*, 14514–14522.

(88) Perdew, J. P.; Burke, K.; Ernzerhof, M. *Phys. Rev. Lett.* **1996**, *77*, 3865–3868.

(89) Güell, M.; Luis, J. M.; Solà, M.; Swart, M. *J. Phys. Chem. A* **2008**, *112*, 6384–6391.

(90) Casiraghi, C.; Hartschuh, A.; Qian, H.; Piscanec, S.; Georgi, C.; Fasoli, A.; Novoselov, K. S.; Basko, D. M.; Ferrari, A. C. *Nano Lett.* **2009**, *9*, 1433–1441.

(91) Neubeck, S.; You, Y. M.; Ni, Z. H.; Blake, P.; Shen, Z. X.; Geim, A. K.; Novoselov, K. S. *Appl. Phys. Lett.* **2010**, *97*, 053110–3.

(92) Wu, J.; Pisula, W.; Müllen, K. *Chem. Rev.* **2007**, *107*, 718–747.

(93) Rieger, R.; Müllen, K. *J. Phys. Org. Chem.* **2010**, *23*, 315–325.

(94) Cai, J.; Ruffieux, P.; Jaafar, R.; Bieri, M.; Braun, T.; Blankenburg, S.; Muoth, M.; Seitsonen, A. P.; Saleh, M.; Feng, X.; Müllen, K.; Fasel, R. *Nature* **2010**, *466*, 470–473.

(95) Schlegel, H. B. *Ab Initio Methods in Quantum Chemistry*; Wiley: New York, 1987; Vol. I.

(96) Boys, S. F.; Bernardi, F. *Mol. Phys.* **1970**, *19*, 553–566.

(97) Costas, M.; Harvey, J. N. *Nat. Chem.* **2013**, *5*, 7–9.

(98) Hirshfeld, F. L. *Theor. Chim. Acta* **1977**, *44*, 129–138.

(99) Wiberg, K. B.; Rablen, P. R. *J. Comput. Chem.* **1993**, *14*, 1504–1518.

(100) Mulliken, R. S. *J. Chem. Phys.* **1955**, *23*, 1833–1840.

(101) Mulliken, R. S. *J. Chem. Phys.* **1955**, *23*, 2343–2346.

(102) van Lenthe, E.; Baerends, E. J. *J. Comput. Chem.* **2003**, *24*, 1142–1156.

(103) Pickering, J. C.; Thorne, A. P. *Astrophys. J. Suppl. Ser.* **1996**, *107*, 761–809.

(104) Kant, A.; Strauss, B. *J. Chem. Phys.* **1964**, *41*, 3806–3808.

(105) Pereiro, M.; Baldomir, D.; Rosales, M. I. C.; Castro, M. *Int. J. Quant. Chem.* **2001**, *81*, 422–430.

(106) Pereiro, M.; Man'Kovsky, S.; Baldomir, D.; Iglesias, M.; Mlynarski, P.; Valladares, M.; Suarez, D.; Castro, M.; Arias, J. E. *Comput. Mater. Sci.* **2001**, *22*, 118–122.

(107) Jamorski, C.; Martinez, A.; Castro, M.; Salahub, D. R. *Phys. Rev. B* **1997**, *55*, 10905–10921.

(108) Wang, H.; Khait, Y. G.; Hoffmann, M. R. *Mol. Phys.* **2005**, *103*, 263–268.

(109) Yanagisawa, S.; Tsuneda, T.; Hirao, K. *J. Chem. Phys.* **2000**, *112*, 545–553.

(110) van Zee, R. J.; Hamrick, Y. M.; Li, S.; Weltner, W. *J. Chem. Phys. Lett.* **1992**, *195*, 214–220.

(111) Hales, D. A.; Su, C. X.; Lian, L.; Armentrout, P. *J. Chem. Phys.* **1994**, *100*, 1049–1057.

(112) Morse, M. D.; Hansen, G. P.; Langridge-smith, P. R. R.; Zheng, L. S.; Geusic, M. E.; Michalopoulos, D. L.; Smalley, R. E. *J. Chem. Phys.* **1984**, *80*, 5400–5405.

(113) Montano, P. A.; Shenoy, G. K. *Solid State Commun.* **1980**, *35*, 53–56.

(114) Parks, E. K.; Klots, T. D.; Riley, S. J. *J. Chem. Phys.* **1990**, *92*, 3813–3826.

(115) Cotton, F. A.; Murillo, C. A. *Multiple Bonds Between Metal Atoms*; Springer: Berlin, 2005.

(116) Mayer, I. *Chem. Phys. Lett.* **1983**, *97*, 270–274.

(117) Yazyev, O. V.; Pasquarello, A. *Phys. Rev. B* **2010**, *82*, 045407–5.

(118) Dai, X.-Q.; Tang, Y.-N.; Zhao, J.-H.; Dai, Y.-W. *J. Phys.: Condens. Matter* **2010**, *22*, 316005–6.

(119) Weisman, J. L.; Lee, T. J.; Salama, F.; Head-Gordon, M. *Astrophys. J.* **2033**, *587*, 256–261.

(120) Kocman, M.; Pykal, M.; Jurećka, P. *Phys. Chem. Chem. Phys.* **2014**, *16*, 3144–3152.

(121) Wohner, N.; Lam, P.; Sattler, K. *Carbon* **2014**, *67*, 721–735.

(122) Buchanan, J. W.; Reddic, J. E.; Grieves, G. A.; Duncan, M. A. *J. Phys. Chem. A* **1998**, *102*, 6390–6394.

(123) Senapati, L.; Nayak, S. K.; Rao, B. K.; Jena, P. *J. Chem. Phys.* **2003**, *118*, 8671–8680.

(124) Pozniak, B. P.; Dunbar, R. C. *J. Am. Chem. Soc.* **119**, *1997*, 10439–10445.

(125) Bendikov, M.; Duong, H. M.; Starkey, K.; Houk, K. N.; Carter, E. A.; Wudl, F. *J. Am. Chem. Soc.* **2004**, *126*, 7416–7417, Erratum in 126, 10493, 2004.

(126) Poater, J.; Bofill, J. M.; Alemany, P.; Solà, M. *J. Phys. Chem. A* **2005**, *109*, 10629–10632.

(127) Horn, S.; Plasser, F.; Müller, T.; Libisch, F.; Burgdörfer, J.; Lischka, H. *Theor. Chem. Acc.* **2014**, *133*, 1511–9.

(128) Jiang, D.; Sumpter, B. G.; Dai, S. *J. Chem. Phys.* **2007**, *126*, 134701–6.

(129) Nagai, H.; Nakano, M.; Yoneda, K.; Kishi, R.; Takahashi, H.; Shimizu, A.; Kubo, T.; Kamada, K.; Ohta, K.; Botek, E.; Champagne, B. *Chem. Phys. Lett.* **2010**, *489*, 212–218.

(130) Jiang, D.; Dai, S. *Chem. Phys. Lett.* **2008**, *446*, 72–75.

(131) Hajgató, B.; Huzak, M.; Deleuze, M. S. *J. Phys. Chem. A* **2011**, *115*, 9282–9293.

(132) Hajgató, B.; Szieberth, D.; Geerlings, P.; Proft, F. D.; Deleuze, M. S. *J. Chem. Phys.* **2009**, *131*, 224321–18.

(133) Rayne, S.; Forest, K. *Comput. Theor. Chem.* **2011**, *976*, 105–112.

(134) Knippenberg, S.; Starcke, J. H.; Wormit, M.; Dreuw, A. *Mol. Phys.* **2010**, *108*, 2801–2813.

(135) Tonshoff, C.; Bettinger, H. *Angew. Chem. Int. Ed.* **2010**, *49*, 4125–4128.

(136) Wang, J.; Zubarev, D. Y.; Philpott, M. R.; Vukovic, S.; Lester, W. A.; Cui, T.; Kawazoe, Y. *Phys. Chem. Chem. Phys.* **2010**, *12*, 9839–9844.

(137) Gross, E. K. U.; Dobson, J. F.; Petersilka, M. *Density Functional Theory*; Springer: Heidelberg, 1996.

(138) Shao, Y.; Head-Gordon, M.; Krylov, A. I. *J. Chem. Phys.* **2003**, *118*, 4807–4818.

(139) Guinea, F.; Neto, A. H. C.; Peres, N. M. R. *Phys. Rev. B* **2006**, *73*, 245426–8.

(140) Yazyev, O.; Helm, L. *Phys. Rev. B* **2007**, *75*, 125408–5.

(141) Casolo, S.; Løvvik, O. M.; Martinazzo, R.; Tantardini, G. F. *J. Chem. Phys.* **2009**, *130*, 054704–10.

(142) Yazyev, O. V. *Phys. Rev. B* **2008**, *101*, 037203–4.

(143) Wu, M.; Liu, E.-Z.; Jiang, J. Z. *Appl. Phys. Lett.* **2008**, *93*, 082504–3.

(144) Boukhvalov, D. W.; Katsnelson, M. I.; Lichtenstein, A. I. *Phys. Rev. B* **2008**, *77*, 035427–7.

(145) Khomyakov, P. A.; Giovannetti, G.; Rusu, P. C.; Brocks, G.; Brink, J. V. D.; Kelly, P. J. *Phys. Rev. B* **2009**, *79*, 195425–12.

(146) Jiménez-Halla, J. O. C.; Robles, J.; Solà, M. *Organometallics* **2008**, *27*, 5230–5240.

(147) Schläfer, H. L.; Gliemann, G. *Basic Principles of Ligand Field Theory*; Wiley Interscience: New York, 1969.

(148) Wehling, T. O.; Lichtenstein, A. I.; Katsnelson, M. I. *Phys. Rev. B* **2011**, *84*, 235110–7.

(149) Wang, J.; Becke, A. D.; Smith Jr., V. H. *J. Chem. Phys.* **1995**, *102*, 3477–3480.

(150) Smalø, H. S.; Åstrand, P.-O.; Jensen, L. *J. Chem. Phys.* **2009**, *131*, 044101–19.

(151) Hu, L.; Hu, X.; Wu, X.; Du, C.; Dai, Y.; Deng, J. *Physica B* **2010**, *405*, 3337–3341.

(152) Mao, Y.; Yuan, J.; Zhong, J. *J. Phys.: Condens. Matter* **2008**, *20*, 115209–6.

(153) Sen, F. G.; Qi, Y.; Alpas, A. T. *J. Phys.: Condens. Matter* **2012**, *24*, 225003–12.

(154) Nakada, K.; Ishii, A. *Solid State Commun.* **2011**, *151*, 13–16.

(155) Thapa, R.; Sen, D.; Mitra, M. K.; Chattopadhyay, K. K. *Physica B* **2011**, *406*, 368–373.

(156) Valencia, H.; Gil, A.; Frapper, G. *J. Phys. Chem. C* **2010**, *114*, 14141–14153.

(157) Ding, J.; Qiao, Z.; Feng, W.; Yao, Y.; Niu, Q. *Phys. Rev. B* **2011**, *84*, 195444–7.

(158) Lima, M. P.; da Silva, A. J. R.; Fazzio, A. *Phys. Rev. B* **2011**, *84*, 245411–6.

(159) Liu, X.; Wang, C. Z.; Yao, Y. X.; Lu, W. C.; Hupalo, M.; Tringides, M. C.; Ho, K. M. *Phys. Rev. B* **2011**, *83*, 235411–12.

(160) Wintterlin, J.; Bocquet, M.-L. *Surf. Sci.* **2009**, *603*, 1841–1852.

(161) Eom, D.; Prezzi, D.; Rim, K. T.; Zhou, H.; Lefenfeld, M.; Xiao, S.; Nuckolls, C.; Hybertsen, M. S.; Heinz, T. F.; Flynn, G. W. *Nano Lett.* **2009**, *9*, 2844–2848.

(162) Evans, J. W.; Thiel, P. A.; Bartelt, M. C. *Surf. Sci.* **2006**, *61*, 1–128.

(163) Gan, Y.; Sun, L.; Banhart, F. *Small* **2008**, *4*, 587–591.

(164) Zhou, Z.; Gao, F.; Goodman, D. W. *Surf. Sci.* **2010**, *604*, L31–L38.

(165) Feibelman, P. J. *Phys. Rev. Lett.* **1987**, *58*, 2766–2769.

(166) Zhang, M.; Li, Y.; Yan, Z.; Jing, J.; Xie, J.; Chen, M. *Electrochimica Acta* **2015**, *158*, 81–88.

Graphical TOC Entry